Table IV. Selected Bond Distances and Angles for $[(C_5Me_5Rh)_2(\mu\text{-}PMe_2)_2(\mu\text{-}Te)]$ (7)

(a) Bond Distances (Å)

Rh(1)···Rh(2)	3.423 (1)	Rh(2)-P(1)	2.295 (3)
Rh(1)-CNT(1)[a]	1.878 (11)	Rh(2)-P(2)	2.284 (2)
Rh(2)-CNT(2)	1.886 (11)	P(1)-C(1)	1.838 (12)
Rh(1)-Te	2.667 (1)	P(1)-C(2)	1.831 (12)
Rh(2)-Te	2.665 (1)	P(2)-C(3)	1.846 (10)
Rh(1)-P(1)	2.288 (3)	P(2)-C(4)	1.823 (11)
Rh(1)-P(2)	2.290 (3)	P(1)···P(2)	2.725 (4)

(b) Bond Angles (deg)

Rh(1)-Te-Rh(2)	79.91 (6)	CNT(2)-Rh(2)-Te	130.3 (1)
Rh(1)-P(1)-Rh(2)	96.6 (1)	CNT(2)-Rh(2)-P(1)	139.1 (2)
Rh(1)-P(2)-Rh(2)	96.9 (1)	CNT(2)-Rh(2)-P(2)	137.2 (2)
CNT(1)-Rh(1)-Te	131.4 (1)	Te-Rh(2)-P(1)	75.2 (1)
CNT(1)-Rh(1)-P(1)	139.1 (2)	Te-Rh(2)-P(2)	75.5 (1)
CNT(1)-Rh(1)-P(2)	136.3 (2)	P(1)-Rh(2)-P(2)	73.0 (1)
Te-Rh(1)-P(1)	75.2 (1)	C(1)-P(1)-C(2)	99.2 (6)
Te-Rh(1)-P(2)	75.3 (1)	C(3)-P(2)-C(4)	99.1 (6)
P(1)-Rh(1)-P(2)	73.1 (1)		

(c) Dihedral Angles (deg)[b]

[P(1)-Rh(1)-P(2)]-[P(1)-Rh(2)-P(2)]	136.7 (3)
[Rh(1)-P(1)-Rh(2)]-[Rh(1)-P(2)-Rh(2)]	127.0 (3)
[Rh(1)-P(1)-Rh(2)]-[Rh(1)-Te-Rh(2)]	116.3 (2)
[Rh(1)-P(2)-Rh(2)-[Rh(1)-Te-Rh(2)]	116.7 (2)

[a] CNT = centroid of Cp* ring. [b] String of atoms in brackets represents the atoms of a plane.

6.59; Rh, 27.52. MS (70 eV): *m/e* 740 (17%; M^+), 725 (100%; $M^+ - CH_3$), 695 (9%; $M^+ - 3CH_3$), 373 (3%; $Rh(C_5Me_5)_2^+$), 238 (3%; $C_5Me_5Rh^+$). ^1H NMR (C_6D_6): δ 3.75 (s; 3 H, CO_2Me), 3.71 (s; 3 H, CO_2Me), 2.31 (d, J_{P-H} = 10.5 Hz, 3 H, PCH_3), 2.00 (d,br, J_{P-H} = 2.6 Hz, 15 H, C_5Me_5), 1.75 (d, J_{P-H} = 10.5 Hz, 3 H, PCH_3), 1.70 (ddd, J_{P-H} = 2.9 Hz, J_{P-H} = 2.1 Hz, J_{Rh-H} = 0.4 Hz, 15 H, C_5Me_5), 1.40 (m, 6 H, PCH_3). ^{31}P NMR (C_6D_6): δ -30.02 (ddd, J_{Rh-P} = 128.8 Hz, J_{Rh-P} = 6.7 Hz, J_{P-P} = 32.8 Hz), -79.84 (ddd, J_{Rh-P} = 142.9 Hz, J_{Rh-P} = 87.8 Hz, J_{P-P} = 32.8 Hz). ^{13}C NMR (C_6D_6): δ 172.20 (s, CO_2Me), 169.61 (s, CO_2Me), 97.39 (s, C_5Me_5), 95.20 (s, C_5Me_5), 49.77 (s, OCH_3), 49.59 (s, OCH_3), 22.48 (s, CCO_2Me), 22.29 (s, CCo_2Me), 14.82 (m, PCH_3), 9.97 (s, $C_5(CH_3)_5$), 9.92 (s, $C_5(CH_3)_5$).

11: yield 105 mg (34%); mp 250 °C dec. Anal. Calcd for $C_{30}H_{48}O_4P_2Rh_2$: C, 48.66; H, 6.53; Rh, 27.79. Found: C, 48.86; H, 6.59; Rh, 27.45. The mass spectra of **11** is almost identical with that of **10**. ^1H NMR (C_6D_6): δ 3.70 (s, 6 H, CO_2Me), 2.26 (vt, N = 11.8 Hz, 6 H, PCH_3), 2.10 (d, J_{Rh-H} = 0.3 Hz, 15 H, C_5Me_5), 1.96 (dt, J_{P-H} = 2.3 Hz, J_{Rh-H} = 0.4 Hz, 15 H, C_5Me_5), 1.40 (vt, N = 7.0 Hz, 6 H, PCH_3). ^{31}P NMR (C_6D_6): δ -2.99 (dd, J_{Rh-P} = 158.3 Hz, J_{Rh-P} = 2.7 Hz). ^{13}C NMR (C_6D_6): δ 173.40 (vt, N = 17.2 Hz, CO_2Me), 96.77 (s, C_5Me_5), 92.18 (d, J_{Rh-C} = 4.5 Hz, C_5Me_5), 50.47 (s, OCH_3), 38.06 (dvt, N = 69.6, J_{Rh-C} = 14.6 Hz, CCO_2Me), 22.81 (dvt, N = 60.9, J_{Rh-C} = 12.1 Hz, PCH_3), 21.60 (s, PCH_3), 11.50 (s, $C_5(CH_3)_5$), 10.80 (s, $C_5(CH_3)_5$).

Crystallographic Structural Determination for 7. Crystals of **7** were grown by layering pentane on a toluene solution. All specimens examined showed extensive interpenetrant twinning; a crystal free of twinning effects was obtained from one arm of a much larger formation. Lattice parameters (Table II) were obtained from the best fit of the angular settings of 25 reflections ($23° \leq 2\theta \leq 30°$). The data were corrected for *Lp* effects, linear decay (~10%), and absorption (empirical, 256 data, ellipsoidal model).

The Te, Rh, and P atoms were obtained by direct methods (SOLV). All nonhydrogen atoms were anisotropically refined, and hydrogen atom contributions were idealized for the (μ-PMe_2) groups but ignored for the C_5Me_5 groups. Table III provides the atomic coordinates and Table IV selected bond distances and angles. SHELXTL software was used for all computations and served as the source for the neutral-atom scattering factors (Nicolet Corp., Madison, WI).

Acknowledgment. We thank the Deutsche Forschungsgemeinschaft and the Fonds der Chemischen Industrie for financial support and Degussa AG for generous gifts of chemicals. We also thank U. Neumann and R. Schedl for the elemental analyses, Dr. G. Lange for the mass spectra, and Dr. W. Buchner and C. P. Kneis for NMR measurements.

Registry No. **2**, 87882-79-9; **3**, 87882-82-4; **4**, 87882-83-5; **5**, 87882-85-7; **6**, 87882-84-6; **7**, 87882-86-8; **8**, 113219-00-4; **9**, 113219-01-5; **10**, 113219-02-6; **11**, 113219-03-7; $C_2(CO_2Me)_2$, 762-42-5.

Supplementary Material Available: Tables of bond distances and angles, anisotropic thermal parameters, and hydrogen atom coordinates (5 pages); F_o/F_c tables (21 pages). Ordering information is given on any current masthead page.

Contribution from the Institut für Anorganische Chemie, Universität Bern, CH-3000 Bern 9, Switzerland, Laboratorium für Kristallographie, Universität Bern, CH-3012 Bern, Switzerland, and Institut de Chimie Minérale et Analytique, Université de Lausanne, CH-1005 Lausanne, Switzerland

Triaqua(benzene)ruthenium(II) and Triaqua(benzene)osmium(II): Synthesis, Molecular Structure, and Water-Exchange Kinetics

Monika Stebler-Röthlisberger,[1a] Wolfgang Hummel,[1b] Pierre-A. Pittet,[1c] Hans-Beat Bürgi,*[1b] Andreas Ludi,*[1a] and André E. Merbach*[1c]

Received September 23, 1987

Solid salts of $M(\eta\text{-}C_6H_6)(H_2O)_3^{2+}$ (M = Ru, Os) are obtained by reacting $[MCl_2(\eta\text{-}C_6H_6)]_2$ with Ag^+ in aqueous solution or by the reaction of $Ru(H_2O)_6^{2+}$ with cyclohexadiene in ethanol. $[Ru(\eta\text{-}C_6H_6)(H_2O)_3]SO_4$ crystallizes in the orthorhombic space group *Pbca* with a = 12.892 (2) Å, b = 12.441 (1) Å, and c = 12.183 (2) Å (T = 125 K), and Z = 8. The structure was refined to 1.9% for 2168 reflections with $F_o > 3\sigma(F_o)$. The relative arrangement of the benzene ring and the three water molecules is approximately staggered, the torsional angle being 19.2 (4)°. After correction for thermal motion, average distances are Ru-C = 2.164 (4), C-C = 1.419 (5), and Ru-O = 2.117 (11) Å. The Ru-center of the benzene plane distance is 1.631 Å. Structural results obtained at 295 K agree with those at 125 K. Water-exchange rates at variable temperature and pressure were determined by line width measurements of ^{17}O NMR spectra at 4.7 T. For $Ru(\eta\text{-}C_6H_6)(H_2O)_3^{2+}$ and $Os(\eta\text{-}C_6H_6)(H_2O)_3^{2+}$ the following results are obtained: k(298 K), 11.5 ± 3.1 and 11.8 ± 2.0 s^{-1}; ΔH^*, 75.9 ± 3.8 and 65.5 ± 2.2 kJ mol^{-1}; ΔS^*, +29.9 ± 10.6 and -4.8 ± 6.1 J K^{-1} mol^{-1}; ΔV^*, +1.5 ± 0.4 and +2.9 ± 0.6 cm^3 mol^{-1}. The reaction proceeds via an interchange mechanism (I) where the bond-breaking contribution has only a slightly larger weight than the bond-making one. The kinetic behavior indicates a strong trans-labilizing influence of the aromatic ligand.

Introduction

Conventional procedures for the preparation of ruthenium arene complexes use the starting reagent "$RuCl_3 \cdot xH_2O$". Bis(arene) species have been originally obtained by treating ruthenium trichloride with an $AlCl_3$/Al mixture and the corresponding arene.[2] An elegant high-yield preparative route to a variety of Ru-arene complexes starts with the reaction of cyclohexa-1,3-diene with "$RuCl_3 \cdot xH_2O$" in ethanol affording the dimeric compound

(1) (a) Institut für Anorganische Chemie, Universität Bern. (b) Laboratorium für Kristallographie, Universität Bern. (c) Université de Lausanne.

(2) Fischer, E. O.; Böttcher, R. *Z. Anorg. Allg. Chem.* **1957**, *291*, 305.

0020-1669/88/1327-1358$01.50/0

$[RuCl_2(\eta^6\text{-}C_6H_6)]_2$.[3-5] Prolonged heating of the analogous *p*-cumene species with an excess of another arene accomplishes complete exchange of the aromatic ligand.[6] These dimeric species serve as precursors to synthesize a large number of monomeric Ru(II) complexes with the general stoichiometry $Ru(\eta^6\text{-arene})L_1L_2L_3$.[7] Depending on pH and anion concentration, treatment of the uncharged dimer in aqueous solution produces ions such as $[\eta^6\text{-arene})Ru(\mu\text{-}X)_3Ru(\eta^6\text{-arene})]^+$ ($X = Cl^-$, OH^-, MeO^-), $Ru(\eta^6\text{-arene})Cl_3^-$, and the cubane-like $[Ru_4(\mu\text{-}OH)_4(\eta^6\text{-arene})_4]^{4+}$.[8] The general aqueous solution chemistry of monomeric η^6-arene complexes of Ru(II) and Os(II) has been summarized by Taube et al., who concluded that the stable species in acidic water occurs as $M^{II}(\eta^6\text{-}C_6H_6)(H_2O)_3^{2+}$.[9]

In the course of our study of the ruthenium aqua ion, we became interested in the $Ru(\eta^6\text{-arene})(H_2O)_3^{2+}$ ion because its combination of ligands represents a unique conceptual link between classical coordination chemistry and organoruthenium compounds. Moreover, this arene–aqua species is a convenient and versatile starting reagent in preparative ruthenium chemistry.[10] A variety of substitution products $Ru(\eta^6\text{-arene})L_3^{2+}$ can be synthesized with L covering a wide range of π-acidity, e.g. Me_2SO, pyridine, $(CH_3)_2S$, and CH_3CN.[11] No member of this novel class of compounds, however, has been fully characterized by its molecular structure or its ligand-exchange properties. It is on this background that we performed a thorough investigation of the $Ru(\eta^6\text{-}C_6H_6)(H_2O)_3^{2+}$ ion encompassing the formation reaction, its crystal and molecular structure, and the water-exchange kinetics in acidic medium as part of a general study concerned with the structure and reactivity of these compounds. The kinetic properties have to be seen in close connection with mechanistic investigation of the water exchange for the hexaaquaruthenium ions.[12]

Experimental Section

A. Preparations and Crystal Growth. The reaction of solid $Ru(H_2O)_6(tos)_2$ (tos = toluenesulfonate)[13a] with cyclohexadiene (the 1,3- or the 1,4-isomer can be used) in EtOH affords orange $[Ru(\eta^6\text{-}C_6H_6)(H_2O)_3](tos)_2$. All crystals investigated by precession photography turned out, however, to be twins. A systematic search for another counterion lead to SO_4^{2-}. The corresponding salt is conveniently prepared from $[RuCl_2(\eta^6\text{-}C_6H_6)]_2$.[4,5] An acidic aqueous solution (pH 1) of this dimer is treated with a stoichiometric amount of Ag_2SO_4. Solid AgCl is removed by filtration. The resulting solution is concentrated by rotatory evaporation at 35 °C until the first orange solid separates; this is redissolved by warming to 50 °C. Slow cooling to 5 °C produces air-stable orange single crystals. Yield: 40%. A further crop can be obtained by repeating the evaporation and cooling. Anal. Calcd for $[Ru(C_6H_6)(H_2O)_3]SO_4$: Ru, 30.7; C, 21.9; H, 3.6; S, 9.7; H_2O, 16.4. Found: Ru, 30.2; C, 21.9; H, 3.7; S, 9.8; H_2O, 16.5.

$[Os(\eta^6\text{-}C_6H_6)(H_2O)_3](tos)_2$ is obtained by dissolving $[OsCl_2(\eta^6\text{-}C_6H_6)]_2$[9] in 1 M Htos and adding a stoichiometric amount of Ag(tos). Filtration of AgCl and concentration of the solution by rotatory evaporation produces a yellow powder. Yield: 88%. Anal. Calcd for $[Os(C_6H_6)(H_2O)_3](tos)_2$: C, 36.1; H, 3.9; S, 9.7; H_2O, 8.1. Found: C, 35.4; H, 4.0; S, 10.0; H_2O, 7.5.

Ru was analyzed spectrophotometrically;[14] elemental analyses were carried out by CIBA-GEIGY, Basel.

B. Crystal Structure Analysis of $[Ru(\eta^6\text{-}C_6H_6)(H_2O)_3]SO_4$. Lattice parameters (Table I) were determined at several temperatures by least-squares optimization of 25 accurately centered reflections in the θ range between 17.5 and 24°. Cell constants decrease linearly with temperature. Intensities were measured at 295 and 125 K on two different crystals with a CAD-4 diffractometer using Mo Kα radiation (graphite monochromator, λ = 0.710 69 Å). For the low-temperature measurements the standard liquid-nitrogen attachment was used. No systematic intensity fluctuations were observed for the three check reflections recorded every 180 min. Intensities were corrected for Lorentz–polarization effects. An empirical absorption correction was applied to the 295 K data by using transmission factors determined experimentally as functions of ϕ. During full-matrix least-squares refinement, neutral-atom scattering factors were employed, including anomalous dispersion for all non-hydrogen atoms.[15] Further details of the data collection and re-

Table I. Crystal Data, Intensity Collection, and Refinement Parameters for $[Ru(\eta^6\text{-}C_6H_6)(H_2O)_3]SO_4$ at 295 and 125 K

	295 K	125 K
space group	*Pbca*	*Pbca*
a/Å	12.919 (2)	12.892 (2)
b/Å	12.501 (2)	12.441 (1)
c/Å	12.282 (2)	12.183 (2)
V/Å^3	1983.5 (5)	1954.0 (5)
fw	329.3	329.3
Z	8	8
D_{measd}(flotation)/g cm^{-3}	2.19 (2)	
D_{calcd}/g cm^{-3}	2.198 (1)	2.239 (1)
cryst dimens/mm	0.2 × 0.15 × 0.1	0.2 × 0.15 × 0.15
linear abs coeff/cm^{-1}	17.6	17.9
2θ limits/deg	1–60	1–60
hkl	≤18,≤17,≤17	≤18,≤17,≤12
scan width/deg	0.8 + 0.4 tan θ	0.8 + 0.35 tan θ
no. of unique reflcns measd	2901	2435
no. of unique reflcns with $F_o > 3\sigma(F_o)$	2509	2168
R/%	2.4	1.9
R_w/%	3.1	3.0
goodness of fit	2.03	2.22
final shift/error (non-hydrogen atoms)	<0.01	<0.01
final shift/error (hydrogen atoms)	<0.2	<0.2

Table II. Final Atomic Positional Parameters and B_{eq} Values, with Standard Deviations in Parentheses, at 125 K[a]

atom	x/a	y/b	z/c	B_{eq}/Å^2
Ru	0.21297 (1)	0.04398 (1)	0.03771 (1)	0.543 (6)
O1	0.2404 (1)	0.1578 (1)	0.1650 (1)	1.19 (4)
O2	0.1110 (1)	−0.0192 (1)	0.1544 (2)	1.51 (4)
O3	0.0867 (1)	0.1440 (1)	−0.0029 (2)	1.46 (4)
C1	0.3654 (2)	−0.0290 (2)	0.0426 (2)	1.62 (6)
C2	0.3689 (2)	0.0640 (2)	−0.0244 (2)	1.61 (6)
C3	0.2993 (2)	0.0770 (2)	−0.1104 (2)	1.76 (6)
C4	0.2235 (2)	−0.0028 (2)	−0.1313 (2)	1.92 (6)
C5	0.2184 (2)	−0.0953 (2)	−0.0660 (3)	2.07 (6)
C6	0.2905 (2)	−0.1083 (2)	0.0215 (2)	1.77 (6)
S	−0.00203 (3)	0.21794 (3)	0.26335 (4)	0.708 (11)
O4	−0.0837 (1)	0.2677 (1)	0.3329 (1)	0.98 (3)
O5	−0.0125 (1)	0.1009 (1)	0.2699 (2)	1.79 (4)
O6	0.1009 (1)	0.2512 (1)	0.3051 (2)	1.72 (4)
O7	−0.0134 (1)	0.2536 (1)	0.1495 (1)	1.71 (4)
H11	0.299 (3)	0.193 (3)	0.165 (3)	2.0[b]
H12	0.195 (3)	0.188 (3)	0.206 (3)	2.0[b]
H21	0.075 (3)	0.019 (3)	0.191 (3)	2.0[b]
H22	0.091 (3)	−0.074 (3)	0.151 (3)	2.0[b]
H31	0.063 (3)	0.174 (3)	0.047 (3)	2.0[b]
H32	0.091 (3)	0.183 (3)	−0.054 (3)	2.0[b]
H1	0.407 (3)	−0.028 (3)	0.111 (3)	2.0[b]
H2	0.414 (3)	0.123 (3)	−0.007 (3)	2.0[b]
H3	0.292 (3)	0.142 (3)	−0.156 (3)	2.0[b]
H4	0.171 (3)	0.011 (3)	−0.188 (3)	2.0[b]
H5	0.160 (3)	−0.150 (3)	−0.067 (3)	2.0[b]
H6	0.283 (3)	−0.154 (4)	0.072 (4)	2.0[b]

[a] $B_{eq} = 8\pi^2/3(U_{11} + U_{22} + U_{33})$; for the numbering scheme, see Figure 3. [b] Fixed values.

(3) Winkhaus, G.; Singer, H. *J. Organomet. Chem.* **1967**, *7*, 487.
(4) Zelonka, R. A.; Baird, M. C. *Can. J. Chem.* **1972**, *50*, 3063.
(5) Bennett, M. A.; Smith, A. K. *J. Chem. Soc. Dalton Trans.* **1974**, 233.
(6) Bennett, M. A.; Matheson, T. W.; Robertson, G. B.; Smith, A. K.; Tucker, P. A. *Inorg. Chem.* **1980**, *19*, 1014.
(7) Bennett, M. A.; Bruce, M. I.; Matheson, T. W. In *Comprehensive Organometallic Chemistry*; Wilkinson, G., Ed., Pergamon: Oxford, England, 1982; Vol. 4, pp 796.
(8) Gould, R. O.; Jones, C. L.; Robertson, D. R.; Tocher, D. A.; Stephenson, T. A. *J. Organomet. Chem.* **1982**, *226*, 199.
(9) Hung, Y.; Kung, W. J.; Taube, H. *Inorg. Chem.* **1981**, *20*, 457.
(10) Bailey, O. H.; Ludi, A. *Inorg. Chem.* **1985**, *24*, 2582.
(11) Stebler-Röthlisberger, M.; Ludi, A. *Polyhedron* **1986**, *5*, 1217.
(12) Rapaport, I.; Helm, L.; Merbach, A. E.; Bernhard, P.; Ludi, A. *Inorg. Chem.* **1988**, *27*, 0000.
(13) (a) Bernhard, P.; Bürgi, H.-B.; Hauser, J.; Lehmann, H.; Ludi, A. *Inorg. Chem.* **1982**, *21*, 3936. (b) Bernhard, P.; Lehmann, H.; Ludi, A. *J. Chem. Soc., Chem. Commun.* **1981**, 1216.
(14) Marshall, E. D.; Rickard, R. R. *Anal. Chem.* **1950**, *22*, 795. Woodhead, J. L.; Fletcher, J. M. *J. Chem. Soc.* **1961**, 5039.
(15) Cromer, D. T.; Waber, J. T. *International Tables for X-Ray Crystallography*; Kynoch: Birmingham, England, 1974; Vol. IV, Table 2.2.B.

Table III. Relaxation Rates, $1/T^b_2$, of the Bound Water ^{17}O NMR Signal of $M(\eta^6\text{-}C_6H_6)(H_2O)_3^{2+}$ at Ambient Pressure and at Different Temperatures in 5–10% ^{17}O-Enriched Water (Composition of the Solutions Given in Figure 1)

M = Ru				M = Os			
T/K	$(1/T^b_2)/s^{-1}$	T/K	$(1/T^b_2)/s^{-1}$	T/K	$(1/T^b_2)/s^{-1}$	T/K	$(1/T^b_2)/s^{-1}$
265.7	4167[a]	358.4	2532	265.1	5514[d]	350.1	1043
273.6	2431	364.2	4208	278.3	3186	355.3	1349
282.2	1768	366.5	4402	294.0	1815	361.8	1742
290.8	1351			301.8	1394	363.3	1910
299.6	1056	330.2	669[b]	311.2	1093	367.9	2513
306.1	905	342.3	966	322.3	896	369.3	2623
319.5	740			333.2	835	373.1	3205
330.7	750	356.1	2135[c]	343.8	844		
342.7	1048	361.7	3101				
348.8	1460	366.7	4691				
353.2	1841						

[a] Solution 1. [b] Solution 2. [c] Solution 3. [d] Solution 4.

finement process are summarized in Table I. The calculations were carried out on a PDP 11/34 computer with the structure determination package of Enraf-Nonius (SDP, version 18) and on a IBM 3033 computer with the PROMETHEUS program system.[16] ORTEP drawings were produced by using the XRAY76 system. Thermal motion analyses were done with the program THMV.[17]

The positions of the non-hydrogen atoms were found by Patterson and Fourier syntheses. After anisotropic refinement of these atoms the positions of the hydrogens were obtained from difference Fourier maps and included in the refinements with fixed isotropic thermal parameters. The function $\sum w(F_o - F_c)^2$ was minimized with $w = 4F^2/[(\sigma(I))^2 + (0.05F^2)^2]$. Final ΔF maps showed residual electron density peaks of +0.63 and −0.77 e/Å^3 in the neighborhood of Ru at 295 K. At 125 K residual densities of 0.30–0.57 e/Å^3 were found on the carbon–carbon bonds, and a residual density of −0.45 e/Å^3 was found near Ru. Final atomic coordinates for the 125 K structure are given in Table II. Listings of the 295 K coordinates, structure factors, and thermal parameters are available as supplementary material.

C. Kinetic Measurements and Determination of Rate Constants. The composition of the four solutions used for the NMR experiments are given in the caption to Figure 1. The solutions were prepared by mixing weighed quantities of the solutes and ^{17}O-enriched water (Yeda, Rehovoth, Israel).

The ^{17}O NMR spectra were recorded with a Bruker CXP-200 spectrometer equipped with a 4.7-T wide-bore cryomagnet working at 27.11 MHz. Ordinary 10-mm NMR sample tubes were used for the variable-temperature measurements. At the highest temperatures the solutions were transferred into totally filled and closed Teflon cells to prevent any change of sample composition due to water evaporation. For the variable-pressure measurements up to 200 MPa a high-pressure probe was used.[18] The temperature was held constant within ±0.2 K (Bruker BVT-1000 unit) by blowing thermostated air (variable temperature) or by pumping a thermostated liquid (variable pressure) through the sample space. Temperature was measured with a substitution technique[19] and a built-in Pt resistor,[20] respectively.

Variable-temperature (-pressure) spectra of 25–36 kHz (25–42 kHz) total width were obtained by Fourier transformation of the free-induction decay (FID) accumulated from no more than 25 000 (40 000) scans. The transverse relaxation rate, $1/T^b_2$ (s^{-1}), of the oxygen resonance of bound water in $[M(\eta^6\text{-}C_6H_6)(H_2O)_3]^{2+}$ (M = Ru, Os) was obtained from the line width at half-height, $\Delta\nu_{1/2}$ (Hz), of its NMR signal least-squares fitted to a Lorentzian curve and from the relation $1/T^b_2 = \pi(\Delta\nu_{1/2})$.

Oxygen-17 enriched aqueous solutions of $[M(\eta^6\text{-}C_6H_6)(H_2O)_3](tos)_2$ (M = Ru, Os) show two ^{17}O NMR signals: a high-intensity one due to bulk water (chemical shift reference) and a small one due to the three water molecules coordinated to the complex (low-frequency shift: Ru = −73.4 ppm, and Os = −66.6 ppm). The exchange rate of the water molecules bound to the diamagnetic complex can be obtained from the observed line width of the ^{17}O resonance of bound water. $Mn(tos)_2$ was added as a relaxation agent to allow accurate measurements of the line width of the bound water signal. The large signal arising from bulk water

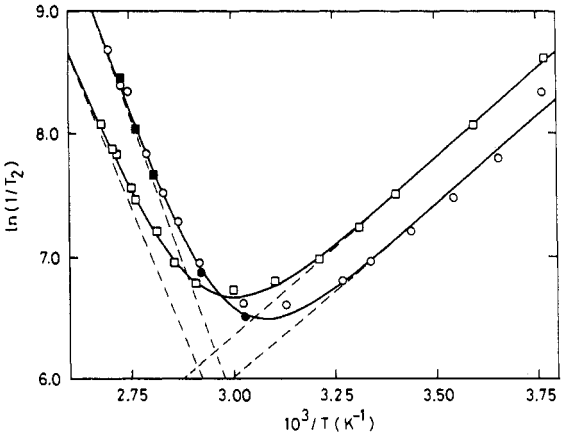

Figure 1. Temperature dependence of the relaxation rates, $1/T^b_2$, of the bound water ^{17}O NMR signal of $M(\eta^6\text{-}C_6H_6)(H_2O)_3^{2+}$ aqueous solutions with the following compositions [solution, M, $[M(\eta^6\text{-}C_6H_6)(H_2O)_3(tos)_2]$ (m), [Htos] (m), $[Mn(tos)_2]$ (m), atom % of $H_2{}^{17}O$]: 1 (○), Ru, 0.60, 1.09, 0.15, 10; 2 (●), Ru, 0.52, 0.98, ..., 5; 3 (■), Ru, 0.59, 0.54, 0.14, 5; 4 (□), Os, 0.59, 1.00, 0.18, 10.

is then suppressed due to very fast water exchange between the bulk and the Mn(II) coordination sphere and due to the long electron relaxation time of this ion. The addition of Mn(II) has no effect on the measured relaxation rates of the diamagnetic metal complex.[21] The very small natural abundance oxygen-17 signal of the counterion tosylate (very slow isotopic exchange) is observed in the Mn(II) solutions at +17.2 ppm.

In the limit of slow exchange,[22] the bound water–^{17}O relaxation rate is given by eq 1, where τ is the mean lifetime of water in the first

$$1/T^b_2 = 1/\tau + 1/T^b_{2Q} \quad (1)$$

coordination sphere and $1/T^b_{2Q}$ is the quadrupolar relaxation rate.

The temperature dependence of $1/\tau$ and its relation to the pseudo-first-order rate constant, k, for the exchange of a particular water molecule[23] and the temperature dependence of $1/T^b_{2Q}$ are given by eq 2 and 3, respectively. The pressure dependence of the exchange rate and of the

$$k = 1/\tau = (k_BT/h)\exp(\Delta S^*/R - \Delta H^*/RT) \quad (2)$$

$$1/T^b_{2Q} = 1/T^b_{2Q}{}^{298}\exp[(E^b_Q/R)(1/T - 1/298.15)] \quad (3)$$

quadrupolar relaxation rate have the form given by eq 4 and 5.[21]

$$\ln k_p = \ln k_0 - \Delta V^*P/RT \quad (4)$$

$$\ln (1/T^b_{2Q})_p = \ln (1/T^b_{2Q})_0 - \Delta V^*_QP/RT \quad (5)$$

Table III summarizes and Figure 1 displays the temperature dependence of the relaxation rates for the ruthenium and the osmium complexes. For $[Ru(\eta^6\text{-}C_6H_6)(H_2O)_3]^{2+}$ the measurements were performed at two different acidities (0.54 and 1.09 m in Htos) to exclude hydrolysis effects on the measured water-exchange rate and in the presence and absence of Mn^{2+} to check the independence of the relaxation rates on the

(16) Zucker, V. H.; Perenthaler, E.; Kuhs, W. F.; Bachmann, R.; Schulz, H. *J. Appl. Crystallogr.* **1983**, *16*, 358.
(17) Trueblood, K. N. *THMV9, Thermal Motion Analysis*; University of California: Los Angeles, CA, 1985. Schomaker, V.; Trueblood, K. N. *Acta Crystallogr., Sect. B: Struct. Crystallogr. Cryst. Chem.* **1968**, *B24*, 63.
(18) Pisaniello, D. L.; Helm, L.; Meier, P.; Merbach, A. E. *J. Am. Chem. Soc.* **1983**, *105*, 4258.
(19) Ammann, C.; Meier, P.; Merbach, A. E. *J. Magn. Reson.* **1982**, *46*, 319.
(20) Meyer, F. K.; Merbach, A. E. *J. Phys. E* **1979**, *12*, 185.
(21) Helm, L.; Elding, L. I.; Merbach, A. E. *Helv. Chim. Acta* **1984**, *67*, 1453.
(22) McLaughlin, A. C.; Leigh, J. S. *J. Magn. Reson.* **1973**, *9*, 296.
(23) Swaddle, T. W. *Advances in Inorganic and Bioinorganic Mechanisms*; Sykes, A. G., Ed.; Academic: London, 1983; Vol. 2, p 121.

Table IV. Relaxation Rates, $1/T^b_2$, of the Bound Water ^{17}O NMR Signal of $M(\eta^6\text{-}C_6H_6)(H_2O)_3^{2+}$ at Different Pressures in 5–10% ^{17}O-Enriched Water (Composition of the Solutions Given in Figure 1)

M = Ru[a]		M = Os[b]			
P/MPa	$(1/T^b_2)$/ s^{-1}	P/MPa	$(1/T^b_2)$/ s^{-1}	P/MPa	$(1/T^b_2)$/ s^{-1}
0.1	2384[c]	0.1	1981[d]	0.1	1394[e]
0.1	2144	0.1	2177	25	1369
25	2048	25	2117	50	1742
55	1968	49	3097	75	1489
75	2022	75	1942	102.5	1470
101	2105	98	2039	125	1473
125	1977	125	1797	148	1505
151	1922	150	1820	174	1497
175	2033	175	1800	201	1477
200	2062	197	1813		

[a] Solution 1. [b] Solution 4. [c] 356.3 K. [d] 360.2 K. [e] 309.7 K.

Table V. Selected Interatomic Distances (Å) and Angles (deg) for $Ru(\eta^6\text{-}C_6H_6)(H_2O)_3^{2+}$

	295 K	125 K	295 K_{cor}	125 K_{cor}
Ru–O1	2.135 (2)	2.130 (1)	2.151 (2)	2.137 (1)
Ru–O2	2.095 (2)	2.090 (2)	2.114 (2)	2.098 (2)
Ru–O3	2.095 (3)	2.105 (1)	2.116 (3)	2.115 (1)
$\langle Ru\text{–}O\rangle_{av}$	2.108 (13)	2.108 (11)	2.127 (12)	2.117 (11)
Ru–C1	2.151 (3)	2.165 (3)	2.178 (3)	2.176 (3)
Ru–C2	2.148 (3)	2.162 (3)	2.174 (3)	2.172 (3)
Ru–C3	2.146 (4)	2.159 (3)	2.170 (4)	2.168 (3)
Ru–C4	2.132 (4)	2.144 (3)	2.153 (4)	2.153 (3)
Ru–C5	2.129 (4)	2.145 (3)	2.151 (4)	2.153 (3)
Ru–C6	2.136 (4)	2.151 (3)	2.160 (4)	2.160 (3)
$\langle Ru\text{–}C\rangle_{av}$	2.141 (4)	2.154 (4)	2.164 (5)	2.164 (4)
C1–C2	1.374 (5)	1.416 (4)	1.404 (5)	1.427 (4)
C2–C3	1.351 (5)	1.388 (4)	1.381 (5)	1.400 (4)
C3–C4	1.395 (6)	1.416 (4)	1.426 (6)	1.427 (4)
C4–C5	1.407 (6)	1.401 (4)	1.437 (6)	1.412 (4)
C5–C6	1.408 (6)	1.423 (4)	1.439 (6)	1.434 (4)
C6–C1	1.393 (5)	1.405 (4)	1.423 (5)	1.415 (4)
$\langle C\text{–}C\rangle_{av}$	1.388 (9)	1.408 (5)	1.418 (9)	1.419 (5)
C_{plane}–Ru	1.629 (1)	1.631 (1)		
C1–C2–C3	121.7 (3)	120.6 (2)		
C2–C3–C4	120.4 (4)	120.0 (2)		
C3–C4–C5	119.6 (4)	120.4 (2)		
C4C5–C6	118.7 (4)	119.2 (2)		
C5–C6–C1	120.0 (3)	120.4 (2)		
C6–C1–C2	119.5 (3)	119.4 (2)		
O1–Ru–O2	82.29 (7)	81.90 (6)		
O2–Ru–O3	83.58 (9)	83.80 (7)		
O3–Ru–O1	83.94 (8)	84.42 (6)		
$\langle O\text{–}Ru\text{–}O\rangle_{av}$	83.3 (5)	83.4 (8)		

added paramagnetic ion. The exchange and NMR parameters listed in Table VI result from least-squares fitting of all these data to eq 1–3, with ΔH^*, ΔS^*, $1/T^b_{2Q}{}^{298}$, and E^b_Q as adjustable parameters. The solid curves in Figure 1 are calculated from these parameters, whereas the dashed lines correspond to the chemical exchange and quadrupolar relaxation contributions.

The variable-pressure $1/T^b_2$ results are summarized in Table IV. For the osmium complex a first series of measurements was performed at 309.7 K. At this low temperature $1/T^b_2$ is due to quadrupolar relaxation only. The data were therefore analyzed by least-squares methods using eq 5. The resulting activation volume ΔV^*_Q for the quadrupolar relaxation is -1.0 ± 0.3 cm^3 mol^{-1} (Table VI). A second series of variable pressure measurements was performed at 360.2 K. This temperature represents a compromise: At lower temperatures the signal to noise ratio would be better, whereas at higher temperatures the unwanted contribution $1/T^b_{2Q}$ ($\sim$20% to $1/T^b_2$) would be smaller. The activation volume, ΔV^*, and the rate constant at zero pressure, k_0, were obtained from a least-squares analysis of the $1/T^b_2$ data using eq 1, 4, and 5 (ln $(1/T^b_{2Q})_0$ and ΔV^*_Q were fixed at the previously determined values).

A similar data treatment was performed for the ruthenium complex (T = 356.4 K). In this case the $1/T^b_{2Q}$ contribution to $1/T^b_2$ is only 10%,

Table VI. Kinetic and NMR Parameters Obtained from Variable-Temperature and Variable-Pressure ^{17}O NMR Bound Water Relaxation Rate of $M(\eta^6\text{-}C_6H_6)(H_2O)_3^{2+}$ (M = Ru, Os)

	M = Ru	M = Os
k^{298}/s^{-1}	11.5 ± 3.1	11.8 ± 2.0
k^{373}/s^{-1}	6770 ± 360	2960 ± 60
ΔH^*/kJ mol^{-1}	75.9 ± 3.8	65.5 ± 2.2
ΔS^*/J K^{-1} mol^{-1}	+29.9 ± 10.6	−4.8 ± 6.1
ΔV^*/cm^3 mol^{-1}	+1.5 ± 0.4[a]	+2.9 ± 0.6[b]
$(1/T^b_{2Q}{}^{298})/s^{-1}$	1120 ± 40	1610 ± 20
E^b_Q/kJ mol^{-1}	23.7 ± 1.2	24.0 ± 5.2
ΔV^*_Q/cm^3 mol^{-1}		−1.0 ± 0.3

[a] At 356.4 K, with k_0 = 1919 ± 65 s^{-1}. [b] At 360.3 K, with k_0 = 1813 ± 48 s^{-1}.

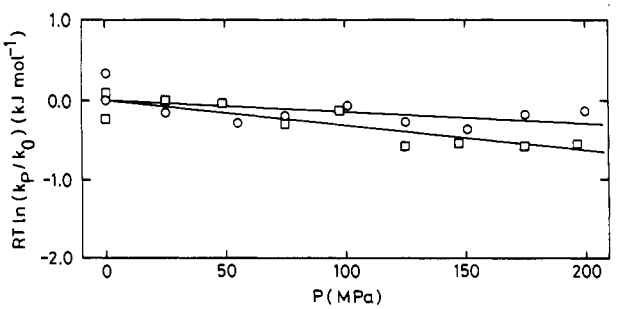

Figure 2. Pressure dependence of the water-exchange rates k_p for $M(\eta^6\text{-}C_6H_6)(H_2O)_3^{2+}$ aqueous solutions (see Figure 1 for the compositions): M = Ru, solution 1 (○) at 356.4 K; M = Os, solution 4 (□) at 360.3 K.

and we have assumed the same ΔV^*_Q as in the osmium case (known ΔV^*_Q values for water bound in different complexes are small: about ±1 cm^3 mol^{-1} [24]). The experimental exchange rates k, obtained after subtraction of $1/T^b_{2Q}$ from $1/T^b_2$, are shown as a function of pressure in Figure 2 (the experimental and calculated k's are normalized to the exchange rate k_0 measured at atmospheric pressure and the respective experimental temperature).

Results and Discussion

A. Formation Reaction and General Properties of $Ru(\eta^6\text{-}C_6H_6)(H_2O)_3^{2+}$. The formation of the dimer $[RuCl_2(\eta^6\text{-}C_6H_6)]_2$ from "$RuCl_3 \cdot xH_2O$" and cyclohexadiene obviously involves a rather complex reaction scheme. By comparison the facile production of an arene complex from $Ru(H_2O)_6^{2+}$ and cyclohexadiene would seem to follow a simpler pathway, apparently conserving the oxidation state of the metal center. Whereas no substitution reaction at all is observed for a mixture of $Ru(H_2O)_6^{2+}$ and benzene in EtOH or MeOH, formation of $Ru(\eta^6\text{-}C_6H_6)(H_2O)_3^{2+}$ is complete within hours at room temperature when cyclohexadiene is employed. When the intensity of the proton NMR signal for the coordinated benzene at 6.1 ppm is used to monitor the reaction, a pseudo-first-order kinetic behavior is observed for about 3 half-lives. The rate for the reaction

$$Ru(H_2O)_6^{2+}\ (0.5 \times 10^{-3}\ M) + C_6H_8\ (20 \times 10^{-3}\ M) \xrightarrow{k} Ru(\eta^6\text{-}C_6H_6)(H_2O)_3^{2+}$$

in THF is $k = 4.6 \times 10^{-4}$ s^{-1} at 303 K. The formation of the arene–aqua complex implies a dehydrogenation process. However, cyclohexene and cyclohexane were detected in the reaction mixture by NMR as well as GC. A disproportionation process would thus seem to be a crucial step in the reaction sequence. Since the signals for C_6H_{10} and C_6H_{12} have approximately equal intensities, the following overall stoichiometry for the formation reaction is proposed:

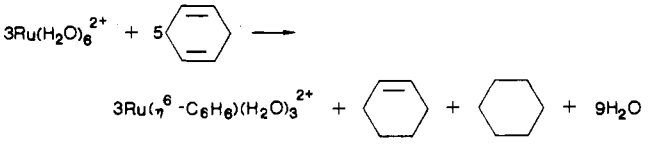

(24) Hugi-Cleary, D.; Helm, L.; Merbach, A. E. *Helv. Chim. Acta* **1985**, *68*, 545.

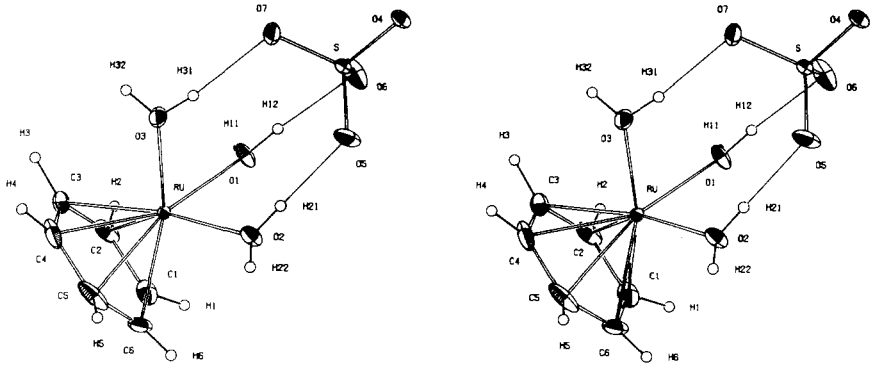

Figure 3. Stereoview of the molecular structure of $Ru(\eta^6\text{-}C_6H_6)(H_2O)_3^{2+}$ and its hydrogen bonds to the SO_4^{2-} anion.

Table VII. Comparison of Kinetic Results

	r(M–O)/Å	k^{298}/s^{-1}	ΔH^*/kJ mol^{-1}	ΔS^*/J K^{-1} mol^{-1}	ΔV^*/cm^3 mol^{-1}
$Ru(H_2O)_6^{2+}$ [a]	2.131	1.8×10^{-2}	88 ± 4	+16 ± 15	−0.4 ± 0.7
$Ru(H_2O)_6^{3+}$ [a]	2.029	3.5×10^{-6}	90 ± 4	−48 ± 14	−8 ± 2
$Ru(H_2O)_5OH^{2+}$ [a]		5.9×10^{-4}	96	+15	+0.9
$Ru(\eta^6\text{-}C_6H_6)(H_2O)_3^{2+}$ [b]	2.127	11.5	76 ± 4	+30 ± 11	+1.5 ± 0.4
$Os(\eta^6\text{-}C_6H_6)(H_2O)_3^{2+}$ [b]		11.8	66 ± 2	−5 ± 6	+2.9 ± 0.6

[a] Reference 12. [b] This work.

Considering the fact that ligand substitution for $Ru(H_2O)_6^{2+}$ with $k = 1.8 \times 10^{-2}$ s^{-1} [12] is 100 times faster than the (pseudo-first-order) formation of $Ru(\eta^6\text{-}C_6H_6)(H_2O)_6^{2+}$, it is not unreasonable to assume that the substitution of one water molecule by one of the olefinic bonds precedes the disproportionation of the organic ligand. Clearly, a more detailed kinetic and mechanistic analysis is required to fully elucidate the reaction pathway. The resulting complex ion with a mixed coordination environment comprising a η^6-benzene and three water molecules can be isolated as air-stable orange-red crystals whose solution in 0.5 M H_2SO_4 shows absorption bands at 400 and 314 nm with extinction coefficients of 550 and 750 M^{-1} cm^{-1}, respectively.

Two independent studies revealed pK_a values of 2.4 (2)[25] and 2.47 (3)[26] for the $Ru(H_2O)_6^{3+}$ ion. For $Ru(H_2O)_6^{2+}$ on the other hand we can only estimate a pK_a of around 6–8. The results of a titration of a $Ru(\eta^6\text{-}C_6H_6)(H_2O)_3^{2+}$ solution with 0.01 M NaOH (ionic strength 0.5; 297.5 K) is compatible with an apparent pK_a = 3.5 (1), rather close to the value for the hexaaqua ion of Ru(III). It must be emphasized, however, that the aqueous chemistry of $Ru(\eta^6\text{-}C_6H_6)(H_2O)_3^{2+}$ is very complex and cannot be described in terms of a simple protonation–deprotonation equilibrium. Possible complications include oligomerization reactions, which are known to occur and which may compete with and obscure the formation of the monomeric hydrolysis product. Various hydroxy-bridged species have been described.[7,8] Solutions of the benzene–aqua ion in 0.5 M H_2SO_4 do not show a reversible signal in the cyclic voltammogram up to 1 V (versus NHE), whereas the reduction potential of the $Ru(H_2O)_6^{3+/2+}$ couple is 0.21 V.[13b] This observation agrees with the π-back-bonding model for ruthenium(II) compounds:[27] The π-acid benzene accepts electron density from the central ruthenium atom to produce a higher charge on the metal; i.e., the $Ru(\eta^6\text{-}C_6H_6)$ moiety behaves like a Ru(III) center. In agreement with this picture, the benzene proton resonances of the ^{1}H NMR spectrum are shifted from 7.27 to 6.1 ppm upon complexation.

B. Molecular Structure of $Ru(\eta^6\text{-}C_6H_6)(H_2O)_3^{2+}$. $Ru(\eta^6\text{-}C_6H_6)(H_2O)_3^{2+}$ shows a "piano-stool" structure with approximate 3 (C_3) symmetry (Figure 3). The benzene ring and the three water molecules are close to a staggered configuration. The average torsional angle O–Ru–ring centroid–C is 23.7 ± 0.2° at 295 K and decreases to 19.2 ± 0.4° at 125 K. The carbon ring is planar; the largest deviation of a carbon atom from the best plane is 0.002 Å at 295 K and 0.003 Å at 125 K. The hydrogen atoms are shifted out of the carbon plane toward the metal. Although the individual shifts lie at the threshold of statistical significance, all shifts are in the same direction and of the same order of magnitude, ≈0.1 Å. Similar results are obtained for dibenzene ruthenium.[28] The C–C distances of the benzene ring show nonsystematic variations at 295 K but significant alternation at 125 K, the average difference between short and long bonds being ≈0.02 Å (Table V). The short distances are trans to the oxygens of the water molecules. The Ru atom is slightly shifted out of the center of the benzene ring toward the C4–C5 bond. The distance from the ring centroid to the projection of the metal onto the carbon plane is 0.03 Å at 295 K and 0.02 Å at 125 K. The variation in Ru–O distances correlates with the variation in Ru–C distances, the longest Ru–O distance being trans to the shortest Ru–C distance and vice versa. The average O–Ru–O angle is 83.3°. The oxygen plane of the water molecules and the carbon plane are slightly tilted with respect to one another. The dihedral angle between the planes is 1.5° at 295 K and 1.6° at 125 K. The H–O–H planes are approximately perpendicular to the benzene and oxygen planes of the complex. This configuration may be due to the intermolecular forces: The three water molecules show almost linear hydrogen bonds to three oxygen atoms of a single SO_4^{2-} anion (Figure 3). The average torsional angle O–S–Ru–O is 1 ± 2° at 295 K and 7 ± 2° at 125 K.

The atoms of the complex cation show elongated displacement tensors that can be interpreted in terms of rotational oscillation about the approximate molecular threefold axis (Figure 3). The cation was treated as a semirigid body in which the benzene ring is allowed additional rotational oscillation about an axis defined by Ru and the centroid of C_6H_6.

The sulfates are connected through hydrogen bonds to the cations. The S–O bond lengths to O4 and O6, both involved in two hydrogen bonds, are more than 0.01 Å longer than those to O5 and O7, involved in one hydrogen only. The corrected average S–O distances are slightly shorter at 125 K than at 295 K. The main libration axis of the SO_4 group is nearly parallel to the main libration axis of the cation. Thus, the three hydrogen bonds between the SO_4 group and the water molecules of the cation result in a strong coupling of the thermal motion of cation and anion.

C. Kinetic Results and Mechanism. The measured exchange for $Ru(\eta^6\text{-}C_6H_6)(H_2O)_3^{2+}$ is 3 orders of magnitude faster than that for $Ru(H_2O)_6^{2+}$ (Tables VI and VII). This is at variance

(25) Harzion, Z.; Navon, B. *Inorg. Chem.* **1980**, *19*, 2236.
(26) Bernhard, P., Ph.D. Thesis, Universität Bern, 1984.
(27) Taube, H. *Surv. Prog. Chem.* **1973**, *6*, 1.
(28) Beck, U.; Hummel, W.; Bürgi, H.-B.; Ludi, A. *Organometallics* **1987**, *6*, 20.

with a straightforward naive application of the back-bonding model, which would predict the exchange rate of the title compound to be in between those of $Ru(H_2O)_6^{2+}$ (1.8×10^{-2} s^{-1} [12]) and $Ru(H_2O)_6^{3+}$ (3.5×10^{-6} s^{-1} [12]). The fast water exchange cannot be attributed to a significant shift of the Ru–O distances either.[29] $Ru(H_2O)_6^{2+}$ and $Ru(\eta^6\text{-}C_6H_6)(H_2O)_3^{2+}$ have very similar thermally corrected (295 K) average metal–oxygen bond lengths of 2.131 (9)[13a] and 2.127 (12) Å, respectively. The very facile substitution of the water ligands in $M(\eta^6\text{-}C_6H_6)(H_2O)_3^{2+}$ should thus be ascribed to transition-state properties rather than to those of the electronic ground state. A similar trans effect in the transition state without corresponding manifestations in structural parameters of the ground state has been discussed for substitution reactions of square-planar platinum(II) complexes.[30]

Activation parameters for the substitution reaction of the two ruthenium aqua ions[12] and the mixed benzene–water complexes are summarized in Table VII. The broad variation of ΔS^* in particular is indicative of distinctively different pathways for the water substitution in the various complex ions. The same conclusion follows from ΔV^*. An interchange mechanism (I) with approximately equal contributions of bond breaking and bond making applies for $Ru(H_2O)_6^{2+}$, the activation volume ΔV^* being -0.4 ± 0.7 cm^3 mol^{-1}. The significantly negative value of ΔV^* (-8.3 ± 2.1 cm^3 mol^{-1}) for $Ru(H_2O)_6^{3+}$ is fully compatible with an associative pathway (I_a).[12] The small positive ΔV^*'s for the two $M(\eta^6\text{-}C_6H_6)(H_2O)_3^{2+}$ complex ions are accepted as evidence for an interchange mechanism in which bond breaking is slightly ahead of bond making. The water-exchange mechanism for these arene–aqua ions is characterized by a strong trans-labilizing effect of the aromatic ligand on coordinated water.

Acknowledgment. We thank CIBA-GEIGY for performing the microanalyses. This work was supported by the Swiss National Science Foundation (Grant No. 2.430-0.84).

Registry No. $Ru(H_2O)_6(tos)_2$, 15694-44-7; $[Ru(\eta^6\text{-}C_6H_6)(H_2O)_3](tos)_2$, 96826-82-3; $[RuCl_2(\eta^6\text{-}C_6H_6)]_2$, 37366-09-9; $[Ru(\eta^6\text{-}C_6H_6)(H_2O)_3]SO_4$, 113221-14-0; $[Os(\eta^6\text{-}C_6H_6)(H_2O)_3](tos)_2$, 113221-15-1; $[OsCl_2(\eta^6\text{-}C_6H_6)]_2$, 69462-16-4; 1,3-cyclohexadiene, 592-57-4; 1,4-cyclohexadiene, 628-41-1.

Supplementary Material Available: Tables SI and SII, listing thermal parameters, Table SIII, listing atomic positional parameters for the 295 K structure, and Table SIV, listing interatomic distances and angles, together with hydrogen bond lengths for the sulfate anion, and Figure 4, the packing diagram of the unit cell (5 pages); tables of calculated and observed structure factors (24 pages). Ordering information is given on any current masthead page.

(29) Bürgi, H.-B.; Dunitz, J. D. *J. Am. Chem. Soc.* **1987**, *109*, 2924.
(30) Tobe, M. L. *Inorganic Reaction Mechanisms*; Nelson: London, 1972; p 50.

Contribution from Department of Inorganic Chemistry 1, Chemical Center, University of Lund, S-221 00 Lund, Sweden

Coordination Chemistry of UO_2^{2+} and VO^{2+} in KSCN–KF Ionic Melts

K. Jarring and B. Holmberg*

Received October 14, 1987

The stepwise complexation of fluoride ions with UO_2^{2+} and VO^{2+} in molten KSCN has been investigated at 185 °C. Fluoride activities were measured in systems (K^+, UO_2^{2+})–(SCN^-, F^-) and (K^+, VO^{2+})–(SCN^-, F^-) by a recently developed potentiometric method utilizing a fluoride-selective membrane electrode. Average ligand numbers from 0 to 4.9 and from 0 to 3.8 were established for the uranyl(VI) and vanadyl(IV) systems, respectively. Higher ligand numbers cannot be achieved due to precipitation of $K_3UO_2F_5$ and K_3VOF_5. Stability constants for five consecutive steps for uranyl(VI) and four consecutive steps for vanadyl(IV) have been determined. A specific interaction energy parameter, ΔA_j, for each step of ligand exchange of thiocyanate for fluoride is determined. For VO^{2+} the overall fluoride complexation is well described by one single parameter: $\Delta A = -39.6$ kJ·mol^{-1}, independent of j for $1 \le j \le 4$. For UO_2^{2+} a slight increase in ΔA_j with increasing j is ascribed to increasing electrostatic repulsion in the equatorial plane of the O–U–O moiety. Changes in hard-sphere Coulomb interaction energies can qualitatively explain the stability sequence $Co^{2+} < Cr^{3+} < VO^{2+} < UO_2^{2+}$ for fluoride complexes in molten KSCN only if formal charges higher than +3.0 and +3.5 are assigned to V and U in VO^{2+} and UO_2^{2+}, respectively. Differences in standard free energy change for the substitution of SCN^- and F^- between aqueous solution (298 K) and KSCN–KF melt (458 K) for these four acceptors are found to be remarkably constant, 29 kJ·(mol F)$^{-1}$, irrespective of central ion and j for $j = 1$ and 2.

Introduction

In recent investigations of fluoride complexation with Cr(III) and Co(II) in molten KSCN, it has been demonstrated that the substitution of SCN^- for the harder ligand F^- in the coordination sphere of the central ion proceeds in a stepwise manner.[1,2] Application of simple quasi-lattice formalism[3] has shown that the specific interaction energy parameters for the ligand-exchange reactions, schematically written as

$$M\text{–}NCS + F^- \rightarrow M\text{–}F + SCN^- \qquad (1)$$

are remarkably constant, i.e. independent of the number of fluoride ions already coordinated to M.

The total complexation from $Cr(NCS)_6^{3-}$ to $Cr(NCS)_2F_4^{3-}$ could thus be modeled by use of one single interaction energy ΔA, once the overall coordination number for the hard acceptor ion Cr(III) was known. These findings of course raise a number of further questions pertaining to complex formation in systems of acceptor–donor pairs of essentially hard–hard character in a fairly soft solvent melt like KSCN. Such questions are as follows: (a) To what extent does F^- associate with other polyvalent metal ions in consecutive steps, which can be described by use of one single quasi-lattice interaction energy parameter? (b) Can observed interaction energies for different acceptor–donor systems be related to estimated changes in hard sphere Coulomb interaction energies in a straightforward way? (c) Is there any relation between thermodynamic parameters for complex formation for hard–hard acceptor–donor pairs in aqueous solution on one hand and molten salts on the other?

In this paper we have extended studies of fluoride systems in KSCN melts to the oxycations UO_2^{2+} and VO^{2+}. These ions have been chosen in order that features in the complexation thermodynamics which may be due to restrictions on the SCN^-/F^- coordination geometry may be detected. UO_2^{2+} and VO^{2+} are probably the two most widely studied oxycations. They are stable in a variety of solvents and give a large number of coordination compounds in the solid state. The complex formation reactions with SCN^- and F^- in aqueous solution are well documented.[4] It

(1) Holmberg, B.; Jarring, K. *Inorg. Chem.* **1987**, *26*, 1713.
(2) Holmberg, B., to be submitted for publication.
(3) Blander, M. *J. Chem. Phys.* **1961**, *34*, 432.
(4) Smith, R. M.; Martell, A. E., Eds.; *Critical Stability Constants*; Plenum: New York, 1976; Vol. 4.

0020-1669/88/1327-1363$01.50/0